Title

Model predictions of deformation, embolization and permeability of partially obstructive blood clots under variable shear flow

Journal

Journal of The Royal Society Interface, 14(136)

ISSN

1742-5689

Authors

Xu, Shixin
Xu, Zhiliang
Kim, Oleg V
et al.

Publication Date

2017-11-01

DOI

10.1098/rsif.2017.0441

Peer reviewed

INTERFACE

rsif.royalsocietypublishing.org

Research

Cite this article: Xu S, Xu Z, Kim OV, Litvinov RI, Weisel JW, Alber M. 2017 Model predictions of deformation, embolization and permeability of partially obstructive blood clots under variable shear flow. *J. R. Soc. Interface* **14**: 20170441.
http://dx.doi.org/10.1098/rsif.2017.0441

Received: 14 June 2017
Accepted: 19 October 2017

Subject Category:
Life Sciences–Mathematics interface

Subject Areas:
biomathematics, biophysics, biomechanics

Keywords:
thrombosis, thromboembolism, blood shear, multi-phase model, multi-scale

Authors for correspondence:
John W. Weisel
e-mail: weisel@pennmedicine.upenn.edu
Mark Alber
e-mail: malber@nd.edu

Electronic supplementary material is available online at https://dx.doi.org/10.6084/m9.figshare.c.3917962.

THE ROYAL SOCIETY PUBLISHING

Model predictions of deformation, embolization and permeability of partially obstructive blood clots under variable shear flow

Shixin Xu[1], Zhiliang Xu[3], Oleg V. Kim[1,4], Rustem I. Litvinov[4,5], John W. Weisel[4] and Mark Alber[1,2,3,6]

[1]Department of Mathematics, and [2]Department of Internal Medicine, Division of Clinical Sciences, School of Medicine, University of California, Riverside, CA 92521, USA
[3]Department of Applied and Computational Mathematics and Statistics, University of Notre Dame, Notre Dame, IN 46556, USA
[4]Department of Cell and Developmental Biology, Perelman School of Medicine, University of Pennsylvania, Philadelphia, PA 19104, USA
[5]Department of Biochemistry and Biotechnology, Kazan Federal University, Kazan 420008, Russian Federation
[6]Department of Medicine, Indiana University School of Medicine, Indianapolis, IN 46202, USA

MA, 0000-0002-7153-1138

Thromboembolism, one of the leading causes of morbidity and mortality worldwide, is characterized by formation of obstructive intravascular clots (thrombi) and their mechanical breakage (embolization). A novel two-dimensional multi-phase computational model is introduced that describes active interactions between the main components of the clot, including platelets and fibrin, to study the impact of various physiologically relevant blood shear flow conditions on deformation and embolization of a partially obstructive clot with variable permeability. Simulations provide new insights into mechanisms underlying clot stability and embolization that cannot be studied experimentally at this time. In particular, model simulations, calibrated using experimental intravital imaging of an established arteriolar clot, show that flow-induced changes in size, shape and internal structure of the clot are largely determined by two shear-dependent mechanisms: reversible attachment of platelets to the exterior of the clot and removal of large clot pieces. Model simulations predict that blood clots with higher permeability are more prone to embolization with enhanced disintegration under increasing shear rate. In contrast, less permeable clots are more resistant to rupture due to shear rate-dependent clot stiffening originating from enhanced platelet adhesion and aggregation. These results can be used in future to predict risk of thromboembolism based on the data about composition, permeability and deformability of a clot under specific local haemodynamic conditions.

1. Introduction

Mechanical stability of intravascular blood clots determines the effectiveness of stemming bleeding (haemostasis) at the sites of vessel injury and the course and outcomes of pathological blood vessel obstruction (thrombosis). Dislodged pieces (emboli) of clots can result in occlusion of downstream blood vessels in lungs or brain, leading to life-threatening complications, such as pulmonary embolism or ischaemic stroke, respectively. Thus, the ability to evaluate and predict the mechanical stability of a blood clot under different flow conditions is necessary for evaluation of the risk of thromboembolism [1]. Mechanical stability of a clot or thrombus and its deformation under blood flow are determined by the structure and mechanical properties of its components [2–7]. Shear flow-induced deformations also change porosity/permeability of a clot, which, in turn, influences the passage of blood components inside the clot. Despite

biological and clinical difficulties, experimental methods have been applied in an attempt to analyse mechanical deformations and embolization of already formed blood clots in response to hydrodynamic forces [2,8–11]. However, experimental studies of *in vivo* clot formation and deformation under blood flow are limited due to inherent methodological difficulties related to selection of biologically relevant thrombosis models, a great number and natural variability of interrelated (patho)physiological parameters, and limitation in resolution of the clot dynamic imaging using intravital microscopy. Therefore, simulations could provide new insights into mechanisms determining clot stability and embolization which are difficult to study experimentally.

A large number of mathematical and computational models have been developed to provide quantitative analysis of blood clot formation and its mechanics [12–17] (for reviews, see [18–21]). In particular, Tomaiuolo *et al*. [11] proposed a model with platelets in clots represented by non-deformable ellipses, and used it to study flow characteristics inside clots. Models described in [11] assumed the structure of the thrombus to consist of a homogeneous porous core and shell domains. Stokes and Brinkman equations were used to simulate blood plasma flow in the lumen region and inside the clot, respectively. These equations were coupled with convection–reaction–diffusion equations describing solute transport in the clot. Fogelson & Guy [22,23] modelled platelet aggregate formation and used evolution equations to compute stresses generated by inter-platelet bonds and demonstrated that shear stress could significantly impact clot growth and its shape through rearrangement of platelets in the clot.

The lattice kinetic Monte Carlo method was introduced in [17] for simulating platelet aggregation in laminar flows and was used to demonstrate that platelet aggregation was enhanced within flow vortices and in narrowing flow regions. A dissipative particle dynamics (DPD) model [24–26] and partial differential equation (PDE) model were combined in a recent paper [27] to simulate clot formation. Platelets were modelled by DPD and the dynamics of fibrin was described by the convection–reaction–diffusion equation. This DPD–PDE hybrid model was used to explore the mechanisms of clot growth. Leiderman & Fogelson [19,28,29] used the PDE modelling approach to study the impact of hindered transport of blood clotting factors on clot formation under flow. They found, due to transport hindrance, a small blood clot that developed in a microchannel had a dense core and a less dense shell structure similar to the clots observed experimentally [10,11,30]. A model with Morse potential was used in the recent paper by Yazdani *et al*. [31] to simulate attractive/repulsive interactions between platelets as well as platelet aggregation under stenosis conditions. Wang *et al*. [32] presented a microscale model of red blood cells (RBCs) and studied in detail dynamics of individual RBCs and platelets. Their simulation results demonstrated that flowing platelets attached mainly to the upstream surface of the clot with no platelet aggregates forming downstream, thus providing a map for platelet–thrombus surface interactions. Additionally, the results of [32] suggested that flow disturbances generated by RBCs were capable of enhancing attachment of platelets to the blood clot surface. A similar approach was used in [33] to graphically represent in real time *in vivo* physiological shear stress environment revealing that clot continuous shape changes were mostly due to its local growth. At the same time, growth or decay dominated in the high shear stress region. A three-dimensional multi-scale model introduced in [34] was used to simulate receptor-mediated adhesion of deformable platelets at the site of vascular injury under different blood flow shear rates. It was shown that platelet deformation, interactions between platelets in the vicinity of the vessel wall as well as the number of functional GPIbα platelet receptors played important roles in platelet adhesion to the injury site.

Despite recent progress in developing biologically relevant models of blood clotting, the roles of structural and mechanical properties of the major clot components such as viscoelastic fibrin network and actively contracting platelets and platelet aggregates have not been addressed in detail. All these clot components actively interact with each other and have a complex and integrative impact on the mechanical stability of a clot. For instance, the fibrin network is known to provide structural and mechanical support for a blood clot and contribute to clot permeability [9]. In addition, platelets actively interact with the fibrin network [35], resulting in clot contraction and an increase in its stiffness. As a result, the permeability of the clot changes during clot remodelling [9]. It has been shown that abnormal clot composition and permeability underlie the instability of clots formed in haemophilic patients or associated with thrombocytopenia and thrombocytosis [9]. Therefore, it is important to develop a comprehensive multi-scale mechanical model of a blood clot for studying and predicting mechanical stability and structural changes of the clot in a highly dynamic environment. Unlike previous papers which focused on simulating formation of a blood clot, the current paper studies the mechanical stability of already formed clots undergoing deformation, as well as their embolization under different shear flow conditions.

This paper starts with the description of the biological background and derivation of a novel two-dimensional (2D) thermodynamically consistent four-component phase-field model of an intravascular blood clot which combines all major clot components and accounts for their interactions. Verification and calibration of the model is then performed by comparing simulations of the flow transport through the clot with experimental data [10,11]. Our model is also verified by calculating the hydrodynamic force acting on the surface of the clot. The relation between the hydrodynamic force and permeability of the shell is shown to be consistent with the previous simulation results [9] (figure 1). The calibrated model is used to study deformations and embolization of a partially occlusive clot developed a few minutes after the injury was created in an arteriole with a diameter of 50 µm [11] under various physiologically relevant flow conditions. While it takes minutes for a clot to form, clot deformation and embolization occurs on a time scale of seconds. The model simulations described in the paper focus on studying these fast dynamical processes. Predictive model simulations have been run for high and low permeable clots (with shell permeability $K_s \geq 5 \times 10^{-12}\,\mathrm{m}^2$ and $K_s < 5 \times 10^{-12}\,\mathrm{m}^2$) and their susceptibility to deformation and embolization have been evaluated. We evaluated the degree of clot deformation for different flow shear rates. Also, previously, the strain-stiffening behaviours of individual fibrin fibres and hierarchical architecture of fibrin fibres were shown to contribute to stiffening of the whole clot [36–39]. Simulations are used to study clot stiffening due to enhanced platelet–platelet adhesive interactions, caused by an increase in the tightness of platelet packing in certain clot regions when the clot interacts with the blood flow.

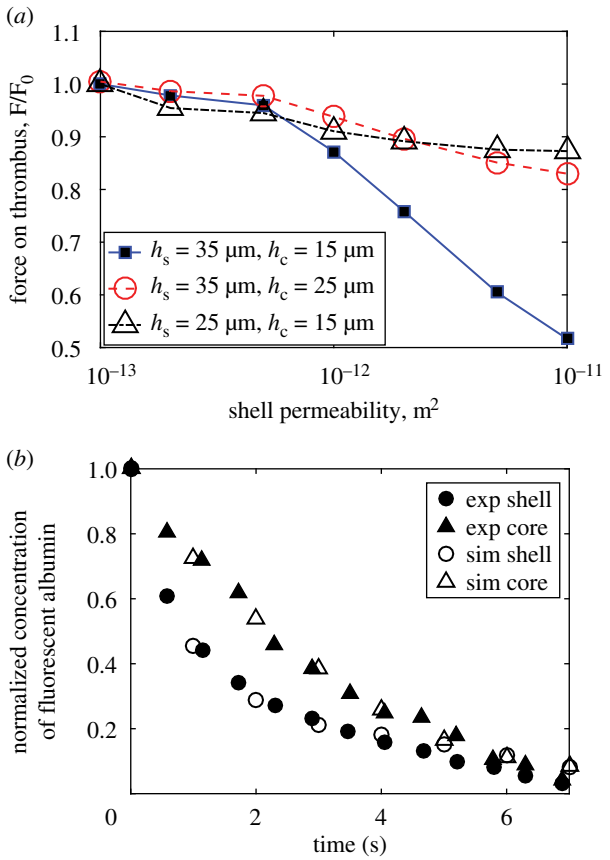

Figure 1. Calibration and validation of the clot model. (*a*) Shear force acting on the surface of the clot as a function of shell permeability, corresponding to different thicknesses of shell and core subdomains of the clot. For each clot thickness, the force is normalized (or divided) by the force acting on the clot with shell permeability 10^{-13} m^2 of the same thickness. h_s and h_c are the thicknesses of the clot and core region of the clot, respectively (figure 3*c*). The relation between the hydrodynamic force acting on the surface of the clot and permeability of the shell region is consistent with the simulation results [9]. (*b*) Time-dependence of the solute concentration due to intra-thrombus flow shown for shell and core compartments of the clot. Solid symbols represent experimental data points [10,11] and open symbols represent the model simulation results. Circles show normalized solute concentration in shell region and triangle symbols correspond to solute concentration in the core. The initial shape of the clot and parameters for transport are the same as in [11]. (Online version in colour.)

2. Background of blood clot formation

To prevent the loss of blood following vessel injury, platelets and various components in the blood and vessel wall interact rapidly to form a blood clot serving as a haemostatic plug. Initially, resting inert platelets in the blood are activated and adhere to each other and to matrix proteins exposed at the site of a vessel injury. Following a sequence of enzymatic reactions [40], thrombin is produced, which activates platelets and converts the soluble protein fibrinogen to insoluble fibrin that forms a filamentous network, the scaffold of a blood clot, providing it with mechanical and lytic stability [41]. The plasma membrane of activated platelets contains the active integrin receptor αIIbβ3 (GPIIbIIIa) that binds fibrinogen and fibrin; fibrinogen bridges adjacent platelets to form aggregates, and fibrin is an adhesive extracellular matrix. Activated platelets change their shape from discoid to star-like with membrane protrusions (filopodia) that facilitate formation of tightly packed cellular aggregates. All the clotting reactions and platelet activation determine the ultimate structure and mechanical properties of the blood clot. The term 'thrombus' designates an intravascular clot that occludes partially or fully a blood vessel, thus blocking the blood flow. When blood clotting and/or platelet activation are impaired, the resulting weak and loose blood clots, if formed, are unstable and prone to mechanical and/or enzymatic disintegration under flow [10,42]. When a piece of a thrombus is torn off and moved downstream it is called an embolus, which can block distant blood vessels, the process termed 'thromboembolism'. (Details about blood clotting, haemostasis and thrombosis can be found in [18,20,43–46].)

3. Description of the multi-phase model of a clot

In the model described in this paper a blood clot or thrombus is assumed, based on experimental studies [10,11], to be composed of a condensed core and a less dense shell region. In the experiments described in [29] intravascular blood clotting was induced in the microcirculation of mouse cremaster muscle by a laser injury of a vessel wall which resulted in development of a partially obstructive clot mainly involving platelet interactions [47]. Although there are limitations related to the control of the depth and extent of the injury which can affect formation of the thrombus, its size and composition [29], the applied laser-induced injury model remains one of the most common minimally invasive experimental thrombosis models. The hardly penetrable core of the clot is formed by fully activated, densely packed platelets and fibrin, whereas the more permeable shell is formed by partially activated, loosely packed platelets [2,10,42,48,49]. To account for the viscoelastic behaviour of the clot components, we adopt a continuum Kelvin–Voigt model, which has been widely used to describe viscoelastic materials with a solid-like behaviour, including biological tissues and fibrin [8,50,51]. In contrast to the model from our previous paper [52], the current model describes flow through a porous clot by using the Brinkman term in the Navier–Stokes equations and takes platelet attachment to and removal from the clot surface into consideration. The convex splitting method and pressure stabilization are used to solve a system of model equations, which is also different from [52]. (The details are provided in the electronic supplementary material.)

3.1. Development of the model

Following the approach developed in [52], generalized Navier–Stokes equations (equations (3.1) and (3.2)) coupled with the Cahn–Hilliard equations (equations (3.3)–(3.5)) are used in our 2D-model to describe blood flow and deformation of a clot consisting of platelets and fibrin. The generalized Navier–Stokes equations are as follows:

$$\nabla \cdot \boldsymbol{u} = 0, \tag{3.1}$$

$$\begin{aligned}\rho(\boldsymbol{u}_t + \boldsymbol{u}\cdot\nabla\boldsymbol{u}) + \nabla P &= \nabla\cdot(\eta \boldsymbol{D}) \\ &- [\lambda_3\gamma_3^2\nabla\cdot(\nabla\phi_3\otimes\nabla\phi_3) + \lambda_2\gamma_2^2\nabla\cdot(\phi_3\nabla\phi_2\otimes\nabla\phi_2) \\ &+ \lambda_1\gamma_1^2\nabla\cdot(\phi_3\phi_2\nabla\phi_1\otimes\nabla\phi_1)] \\ &- (\nabla\cdot(\lambda_e\nabla\Psi^{\mathrm{T}}\nabla\Psi)) - \frac{\eta\phi_3}{\kappa}\boldsymbol{u}\,.\end{aligned} \tag{3.2}$$

Cahn–Hilliard equations yield

$$\partial_t\phi_1 + \nabla\cdot(\boldsymbol{u}\phi_1) = \nabla\cdot(M_1\nabla\mu_1), \tag{3.3}$$

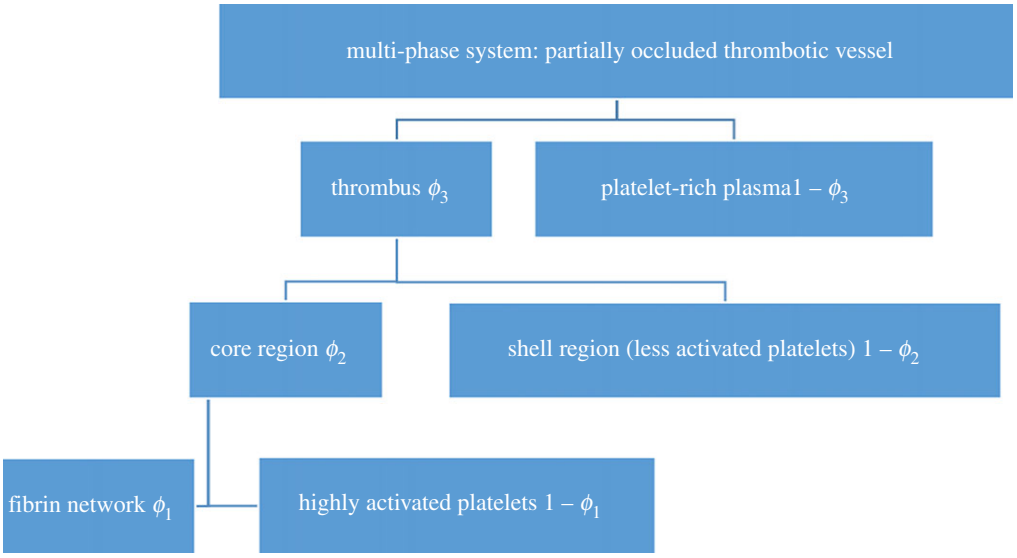

Figure 2. Diagram of the multi-phase model of a clot indicating interactions between all basic components of the clot represented by phase volume fractions. ϕ_3 is the volume fraction of the clot (figure 3*b*), plasma has volume fraction $(1 - \phi_3)$. The low porosity core region (in red, figure 3) is represented by the volume fraction $\phi 2$ and the high porosity shell region (in green, figure 3) has volume fraction $(1 - \phi_2)$. Volume fractions of fibrin and highly activated platelets in the core of the clot are ϕ_1 and $(1 - \phi_1)$, respectively.

$$\partial_t \phi_2 + \nabla \cdot (\boldsymbol{u}\phi_2) = \nabla \cdot (M_2 \nabla \mu_2) \tag{3.4}$$

$$\partial_t \phi_3 + \nabla \cdot (\boldsymbol{u}\phi_3) = \nabla \cdot (M_3 \nabla \mu_3) + S_g. \tag{3.5}$$

Here, $\boldsymbol{u}$, P and ρ are complex fluid velocity, pressure and density, respectively. ϕ_1 is the volume fraction of fibrin network in the core region, ϕ_2 is the volume fraction of the core region in the clot, and ϕ_3 is the volume fraction of the clot as a part of the entire complex fluid (figure 2). $\eta(\phi_1, \phi_2, \phi_3)$, $\lambda_e(\phi_1, \phi_2, \phi_3)$ and $\kappa(\phi_2)$ are viscosity of the complex fluid, elasticity and permeability of the clot, respectively. (see section A.1 of the electronic supplementary material for their definitions.) Also, η and λ_e are functions of volume fractions ϕ_1, ϕ_2, ϕ_3, and κ is a function of ϕ_2. Phase-field method parameters λ_i, γ_i and M_i denote mixed energy density, capillary width and phenomenological mobility coefficient of ϕ_i for $i = 1,2,3$, respectively. $\boldsymbol{\Psi}$ is a vector used to describe the elasticity of the clot. The first term on the right-hand side of equation (3.2) represents viscosity force with $\boldsymbol{D} = (\nabla \boldsymbol{u} + (\nabla \boldsymbol{u})^{\mathrm{T}})$. Three terms in the square breakets are the adhesion forces due to interaction between different clot components. The fifth term $\nabla \cdot (\lambda_e \nabla \Psi^{\mathrm{T}} \nabla \Psi)$ represents elastic force generated by the clot in response to deformations, and the last term is the Brinkman term related to flow through a porous clot (see electronic supplementary material, equation (A 17)).

Chemical potentials μ_i, $i = 1,2,3$ [53], used to describe interactions between different components, are defined as follows:

$$\mu_1 = \lambda_1(\phi_2\phi_3 G_1'(\phi_1) - \gamma_1^2 \nabla \cdot (\phi_2\phi_3 \nabla \phi_1)) + \frac{\partial_1 \lambda_e}{2} |\nabla \Psi|^2,$$

$$\mu_2 = \lambda_2(\phi_3 G_2'(\phi_2) - \gamma_2^2 \nabla \cdot (\phi_3 \nabla \phi_2)) + \lambda_1 \left(\phi_3 G_1(\phi_1) + \gamma_1^2 \phi_3 \frac{|\nabla \phi_1|^2}{2} \right) + \frac{\partial_2 \lambda_e}{2} |\nabla \Psi|^2$$

and

$$\mu_3 = \lambda_3(G_3'(\phi_3) - \gamma_3^2 \Delta \phi_3) + \lambda_1 \phi_2 \left(G_1(\phi_1) + \gamma_1^2 \frac{|\nabla \phi_1|^2}{2} \right) + \lambda_2 \left(G_2(\phi_2) + \gamma_2^2 \frac{|\nabla \phi_2|^2}{2} \right) + \frac{\partial_3 \lambda_e}{2} |\nabla \Psi|^2.$$

Here, ∂_i denotes ∂_{ϕ_i}, $i = 1,2,3$. G_i denotes free energy functional [54]. (The explicit form of G_i is provided in the electronic supplementary material.)

To model interactions of platelets freely flowing in the blood with a clot surface (i.e. cohesion with partially activated adherent platelets) via formation and breakage of αIIbβ3-fibrinogen bonds [55,56], we introduce a phenomenological submodel using function $S_g(\boldsymbol{x}, t)$ that describes fluxes of platelets during attachment to and detachment from the surface of the blood clot (see electronic supplementary material, equation (A 13)).

Derivation of equations (3.1)–(3.5) is based on the energetic variational approach (see [2,3] in the electronic supplementary material). An efficient numerical algorithm is developed to solve equations (3.1)–(3.5) which uses pressure stabilization method for the Navier–Stokes equations and convex splitting method for the Cahn–Hilliard equations. (Details of the numerical scheme and its implementation are given in the electronic supplementary material, A.5. The code is written by using the platform FreeFem [57].)

3.2. Model assumptions and parameters values

The parameter values used in the model simulations are listed in table 1. The assumption of the initial two-component core–shell structure of the blood clot is based on the intravital light microscope images of an arteriolar clot in a mouse [10]. Initial distributions of platelets and fibrin within the simulated clot are based on the experimental observations [10,11,42,49]. Unless otherwise noted, the relative volume fractions of the dense matter and liquid plasma in a clot are assumed to be 0.7 and 0.3, respectively, in the core region and 0.3 and 0.7,

Table 1. Parameter values used in simulations.

notation	description	value
ρ	plasma density	1.025 kg m^{-3} [58]
η_f	viscosity of plasma	4 cP [16]
η_n	shear viscosity of fibrin network	400 cP (estimated from [59])
η_p	shear viscosity of aggregate of highly activated platelets	2000 cP (estimated from[59])
η_r	shear viscosity of aggregate of less activated platelets	100 cP (estimated from[59])
K_c	permeability of core region	10^{-13}–10^{-15} m^2 [11,60]
K_s	permeability of shell region	10^{-11}–10^{-13} m^2 [60,61]
λ_n	dynamic elastic modulus of fibrin network	4 Pa (estimated from [3,62])
λ_p	dynamic elastic modulus of highly activated platelet aggregates	40 Pa (estimated from [62])
λ_r	dynamic elastic modulus of less activated platelet aggregate	4 Pa (estimated from [62])
λ_i	mixed energy density of different phase (constant)	400 Pa (estimated from [62])
k_n	accumulation coefficient	0.02 cP (estimated from [10])
k_g	detachment coefficient	0.2 cP (estimated from [10])
γ_i	mixing interface width	1 μm (estimated)
τ_i	ith component's mobility	2.5×10^{-9} sm^3/kg (estimated)

respectively, in the shell region (figure 3*b*). Fibrin is assumed to be present only in the core region [10]. A computational domain is set to be [0–300 μm] × [0–50 μm] for the blood clot simulations as shown in figure 3*c*. The mesh size $h = 0.78$ μm and the time-step size $\mathrm{d}t = 10^{-5}$ s are used for spatial and temporal discretization in all simulations. RBCs were not present in the small (30–50 μm) clot in the experiements in [10] and were not considered in our simulations either.

4. Model verification and calibration

4.1. Shear force on the blood clot surface

The model was first verified by calculating the total shear force acting on the clot surface defined as $F_v = \left| \int_S \boldsymbol{v} \cdot \eta(\nabla \boldsymbol{u} + (\nabla \boldsymbol{u})^{\mathrm{T}}) \cdot \boldsymbol{n}\, \mathrm{d}s \right|$ and comparing it with the simulation results of the Darcy–Stokes–Brinkman flow model from [9]. Here $\boldsymbol{n}$ and $\boldsymbol{v}$ are the unit normal and tangential vectors to the clot surface S. The initial structure of the simulated clot is shown in figure 3*b*. The permeability of the core region of the clot was taken as 10^{-14} m^2 [60,61]. Figure 1*a* shows the total shear force for seven values of permeability of the shell region. To verify the model, we calculated the force on the clot having the following core and shell size (h_s, h_c) [9]: (35 μm, 15 μm), (35 μm, 25 μm), (25 μm, 15 μm), where h_s and h_c are the height of the entire clot and the core region, respectively. For model verification we assume that the shape and distribution of the clot does not change, i.e. we solve the Navier–Stokes equations without modifying ϕ_i. In all simulations, the total shear force decreased monotonically as the permeability of the shell region increased. In particular, for the 35 μm thick clot with 15 μm thick core, the shear force reduced from 170 to 88 Pa when the permeability increased from 10^{-13} to 10^{-11} m^2. This is consistent with the earlier obtained simulation results [9]. For a large clot with a small core ($h_s = 35$ μm, $h_c = 15$ μm), there is a sharp decrease of force with increase in permeability. In this case, there is a relatively thick shell region where the permeability is higher than the permeability of the core region, allowing plasma to flow through the shell. As the permeability increases, the difference between velocities outside and inside of the clot decreases, which in turn, reduces the shear force acting on the clot surface.

4.2. Solute transport inside a clot

The model was then calibrated by computing transport of albumin through the clot and comparing the simulation results with the experimental data [10,11]. The initial core-and-shell structure of the clot was assumed to be the same as the one observed in the experiment [11]. The diffusion coefficients of albumin in the core and shell regions as well as in bulk plasma were taken as 4×10^{-12} m^2 s^{-1}, 10^{-11} m^2 s^{-1}, and 6×10^{-11} m^2 s^{-1}, respectively [11]. Porosities of the core and shell regions were taken to be 0.2 and 0.4, respectively (Table 2 of [11]), which corresponded to the initial clot volume fractions in the core and shell regions of 0.8 and 0.6, respectively. The permeabilites of the shell and core regions were set to the typical values of 1×10^{-13} m^2 and 10^{-15} m^2, respectively [61]. The maximum inlet flow velocity was $\boldsymbol{u}_{\max} = 2 \times 10^{-3}$ m s^{-1} [11]. To compute albumin transport, the convection–diffusion equation $(\partial c/\partial t) + \boldsymbol{u} \cdot \nabla c = D\Delta c$ was solved with $c = 0$ at the inlet boundary. Here c is the albumin concentration. The final time for the simulation results shown in figure 1*b* is 7 s. The calculated changes in albumin concentration inside the clot over time were in agreement with experimental data on temporal dynamics of albumin concentration, which was quantified in terms of albumin fluorescence intensity (figure 1*b*). Thus, our model correctly describes solute transport and can be used to simulate flow hindrance induced by the clot structure.

4.3. Calibration of the rate function S_g

Experiments showed that free-flowing platelets first attached to the upstream side of the clot surface, moved along the clot surface, and were then removed by the flow from the clot surface

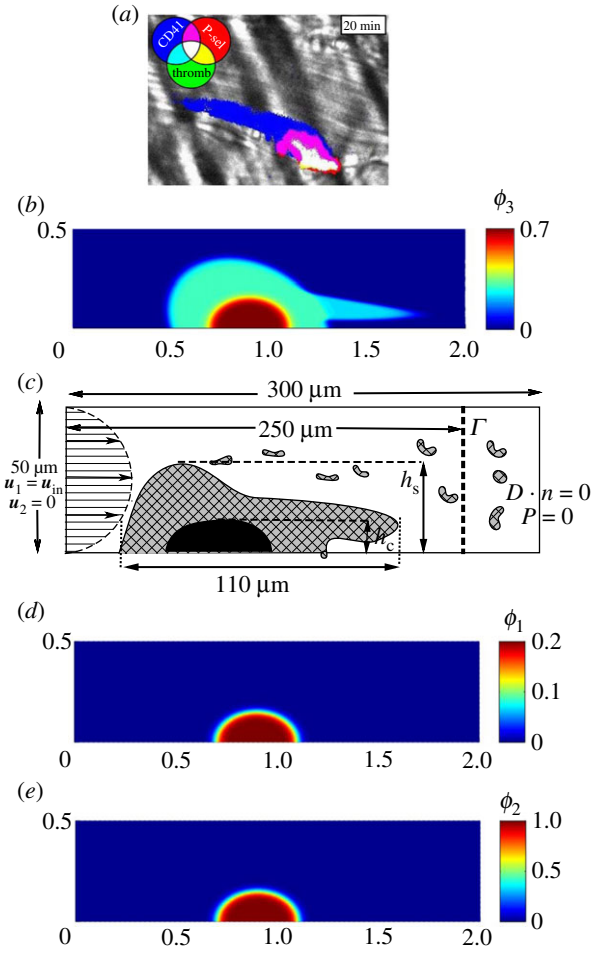

Figure 3. The initial structure of an arterial blood clot used in simulations. (*a*) A snapshot of the experimental movie of a blood clot at about 20 min after injury (fig. 5a in [10], reproduced with permission from the journal). (*b*) The initial structure of a simulated blood clot in terms of the clot volume fraction ϕ_3. The core of the clot consisting of highly activated platelet aggregates and fibrin network is shown in red, and the clot shell region comprising less activated platelet aggregates is shown in light-green. The dark blue region around the clot corresponds to plasma flow ($\phi_3 = 0$). (*c*) Schematic diagram of the computational domain, flow boundary conditions and the location of the platelet counting section (dashed border line, Γ) used to calculate the clot fragmentation rate. A constant inlet flow is specified at the left boundary and an open flow boundary condition is used at the right boundary. Here $\boldsymbol{u}_1$ and $\boldsymbol{u}_2$ are the longitudinal and normal velocities, along and perpendicular to the vessel wall, respectively, p is the pressure, h_s and h_c are the thicknesses of the clot and its core region, respectively. We assume the inlet flow profile is described by $u_{in} = 16(0.5 - y)yu_{max}$ where u_{max} is the flow velocity at the middle of the vessel. (*d*) The initial structure of the simulated core region fraction in the clot ($\phi_2(t = 0)$). (*e*) The initial structure of the fibrin network fraction in the core region ($\phi_1(t = 0)$). (Online version in colour.)

at the downstream side [55]. These platelet–clot surface interactions are described in the model by the rate function S_g (see electronic supplementary material, equation (A9)), based on the assumption that platelet attachment to and removal from the clot surface are driven by the normal and tangential flow stress components. The accumulation k_n and detachment coefficients k_v in S_g are chosen to balance the amount of platelets accumulated on and detached from the clot surface under a low shear rate (500 s^{-1}). The calculated distribution of the S_g magnitude over the clot surface is shown in figure 4*a*. It is consistent with the experimental observations [10] (figure 4*b*),

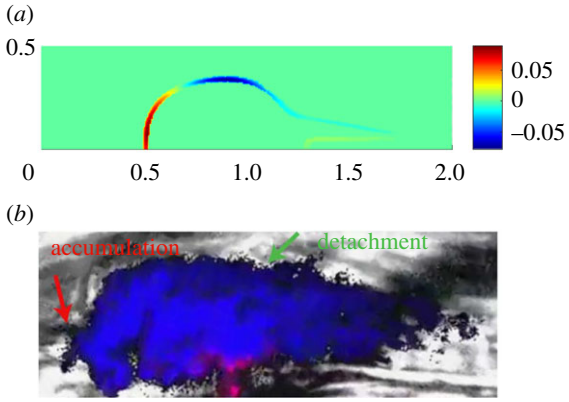

Figure 4. Accumulation and detachment of free-flowing platelets over the surface of the blood clot. (*a*) Simulated distribution of the magnitude of the rate function S_g (s^{-1}) on the surface of the blood clot with shell permeability $K_s = 10^{-12}$ m^2 at shear rate $\dot{\gamma} = 1000$ s^{-1}. Platelet accumulation on the upstream surface of the clot is shown by the red zone. Platelet detachment zone on the clot surface is shown in blue. The unit of length is $L =$ 100 μm (figure 3*c*). (*b*) A snapshot of the experimental movie showing the arterial clot formed *in vivo* (movie is provided as a supplementary information to [10]). Small dots indicate single platelets. Arrows show the locations of platelet accumulation on the upstream surface of the clot and of platelet detachment from the top portion of the clot surface. The region with platelet aggregates is indicated in blue colour and the domain with fibrin network in the core of the clot is indicated in red colour. (Online version in colour.)

which revealed accumulation of platelets on the upstream part of the clot surface where the flow shear stress reaches its minimum. Namely, the free-flowing platelets are transported towards this part of the clot surface by the flow and subsequently accumulate there.

At the same time, weakly attached platelets and platelets aggregates are moved by the flow along the clots exterior and can detach from the top surface of the clot where the shear stress reaches its maximal value. As a result, platelets encountering the upstream part of the clot get attached to its surface whereas partially activated superficial platelets located downstream, in the zone of a higher flow shear stress, are peeled off the clot. Although transient flipping and rolling behaviour of individual platelets is not considered in the current model, the approach, similar to one described in [32], can be applied for a more detailed description of platelet-clot interactions involving platelet αIIbβ3 integrin–fibrin(ogen) pairs [34,63].

5. Simulation results and discussion

Changes in size and shape of a 35 μm blood clot formed in a 50 μm diameter blood vessel were simulated under physiological shear rates corresponding to the arteriole blood flow from $\dot{\gamma} = 250$ to 2000 s^{-1} [64,65] with clot permeability levels ranging from 10^{-14} to 10^{-11} m^2. Degree of clot deformation and total size of dislodged clot pieces (emboli) were calculated to quantify the shear-induced changes.

5.1. Effect of the variable flow shear on clot deformation

Simulations indicated significant deformations of the clot shell accompanied by redistribution of partially activated

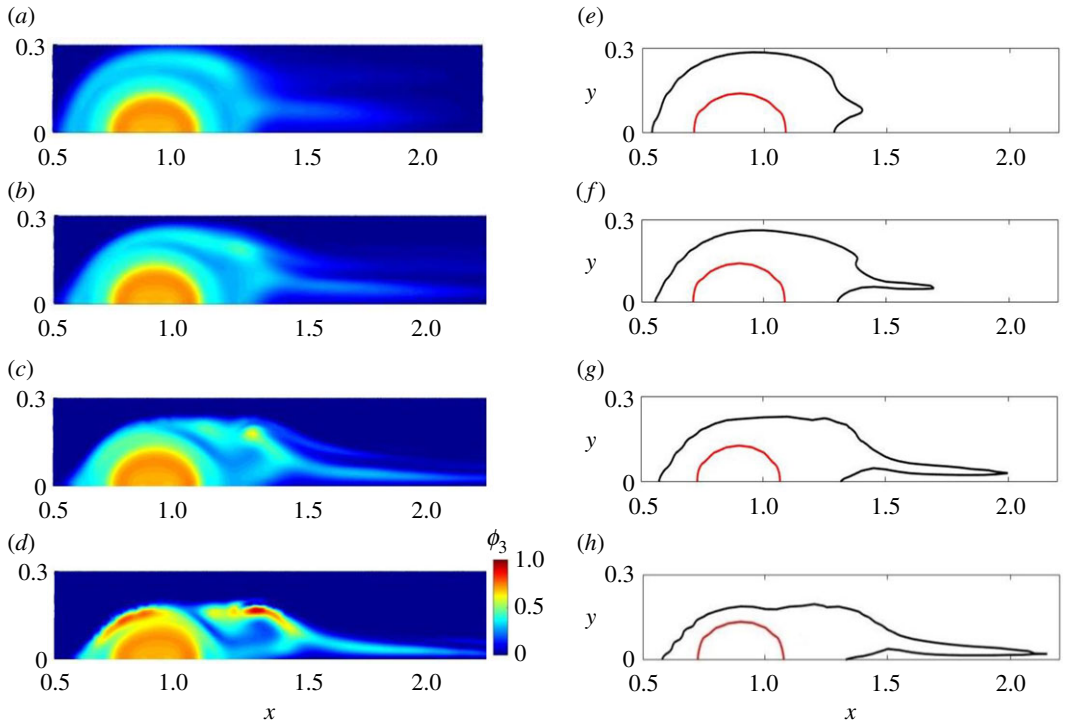

Figure 5. Impact of the flow shear rate on blood clot stability. (*a–d*) Spatial distributions of clot volume fraction at different shear rates: $\dot{\gamma} = 250\ s^{-1}$ (*a*), $500\ s^{-1}$ (*b*), $1000\ s^{-1}$ (*c*), $2000\ s^{-1}$ (*d*), at time $t = 0.2$ s. (*e–h*) Deformation patterns of a blood clot corresponding to (*a–d*). The black line outlines the blood clot surface; the red line shows the interface between the core and shell regions. The length unit is $L = 100$ μm (figure 3*c*). (Online version in colour.)

surface-attached platelets at different shear rates (figure 5). As the flow rate increased platelet aggregates comprising the shell region of the clot were gradually pushed by the flow to the downstream side of the clot. At a flow rate of $2000\ s^{-1}$ most of the platelets in the shell were translocated downstream, forming elongated filament-like aggregated multicellular structures (figure 5*d*,*h*). Meanwhile, the core of the clot retained its shape (red line) over the applied range of flow shear rates. These results are in good agreement with the experimental observations [10,42], indicating formation of a tear-like elongated structure under flow formed from a clot that consisted of an undeformable core and flexible shell region (fig. 4a in [10]).

5.1.1. Degree of clot deformation as a function of shear rate

To quantify clot deformability, the degree of clot deformation was defined in terms of the clot volume-averaged deformation gradient tensor (DGT) as $\langle \mathbf{F} \rangle = \int_{\Omega_c} \left(\sum_{i,j=1,2} \mathbf{F}_{ij}^2 \right)^{1/2} d\boldsymbol{x}/\mathrm{Vol}_c$, where $\mathrm{Vol}_c = \int_{\Omega_c} \phi_3 d\boldsymbol{x}$ is the volume of the blood clot, Ω_c is the blood clot domain, and $\mathbf{F} = \partial \boldsymbol{x}/\partial \mathbf{X}$ is the DGT which characterizes shape changes of a clot with respect to its initial configuration. Here $\boldsymbol{x}$ and $\mathbf{X}$ are the current and original coordinates. (see electronic supplementary material, A.1.)

Our simulations revealed that the degree of deformation in the clots increased non-linearly by approximately 50% as the shear rate increased from 250 to $1000\ s^{-1}$ and remained constant at the higher shear rates (figure 6*a*). Shear rates indicated in figure 6*a* by the square symbols are equal to the maximum shear rate at the inlet. Figure 6*a* indicates the strain-stiffening behaviour of a clot during deformation, as revealed by the stress-deformation relation (figure 6*b*). The model predicts that this strain-stiffening is attributed to an increase of platelet density (i.e. tight packing followed by a decrease of porosity, see figure 7*a*) in the shell of the clot.

5.1.2. Time-dependence of clot deformation under shear

Time dependence of the degree of deformation of the blood clot expressed as the average DGT norm is shown in the inset in figure 6*a*. It demonstrates that there are two shear rate-dependent super-linear and saturation regimes of clot deformation over time, with the super-linear portion being shorter for the higher shear rates. As the shear rate increases from 1000 to $2000\ s^{-1}$, the onset of nonlinear deformation shifts from 0.2 to 0.1 s. Transition from the linear to nonlinear regimes can be attributed to cessation of clot deformation as the hydrodynamic force and the mechanical resistance of the clot balance each other.

5.1.3. Spatial non-uniformity of clot hydrodynamics

Our simulation results show a spatially non-uniform distribution of plasma velocity inside the clot with a mean flow speed within the clot shell being four orders of magnitude higher than that inside the core and an order of magnitude lower than the plasma flow speed outside the clot (figure 6*d*). The mean flow speed inside the shell was quite insensitive to changes of the external flow, remaining around $0.1\ cm\ s^{-1}$ even at the highest free-flow speed of $2.5\ cm\ s^{-1}$, emphasizing the role of clot porosity in hindering the flow, which was in agreement with previous studies on thrombus internal transport [11]. Our simulations revealed a nonlinear increase of the mean flow speed in the shell domain as the flow speed outside the clot increased which is in contrast with the previously published data [11] showing a linear relation between the internal and external flow

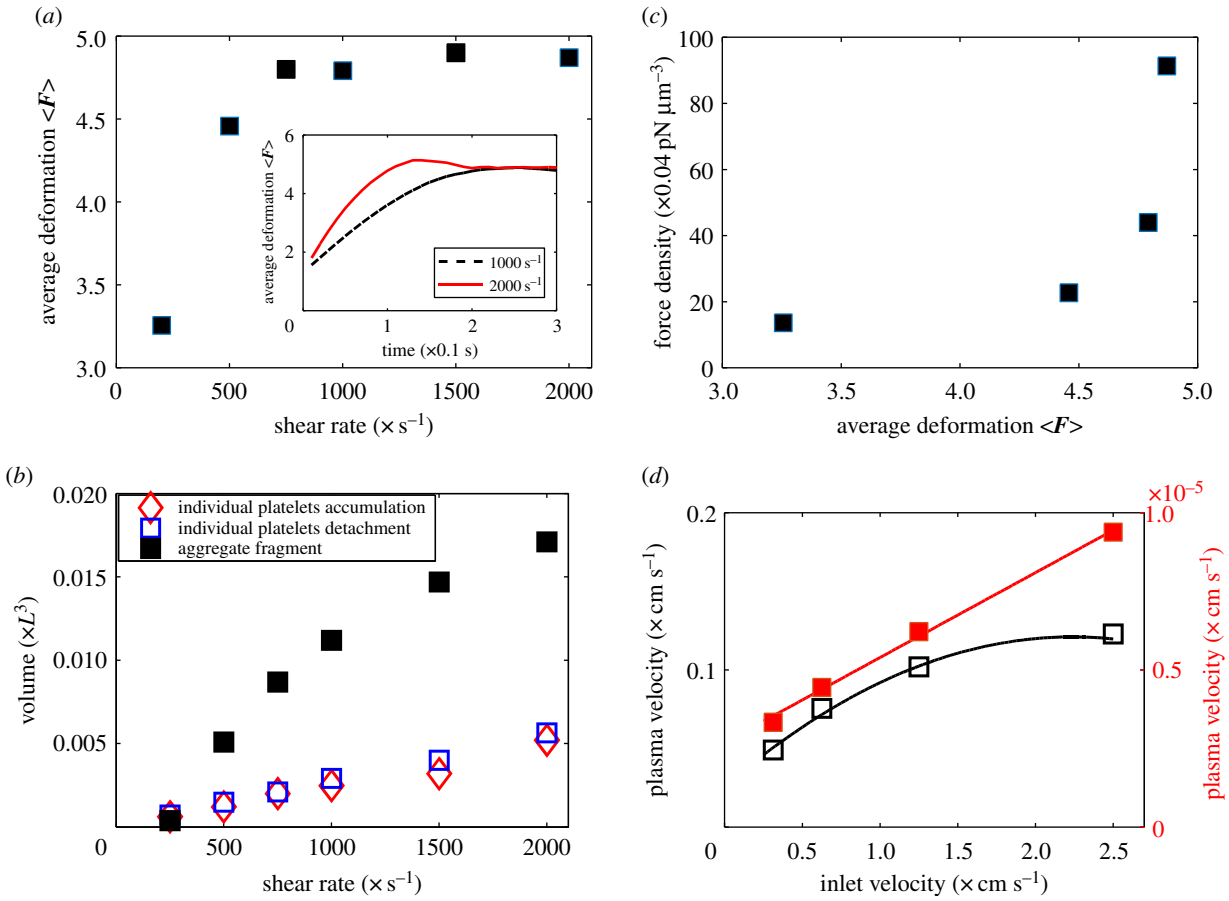

Figure 6. Impact of the flow shear rate on blood clot deformation and disintegration dynamics (*a–c*). (*a*) Clot deformation degree in terms of the average deformation tensor norm $\langle \boldsymbol{F} \rangle$ for different shear rates. The shear rates indicated by the square symbols are equal to the maximum shear rate at the inlet. The inset shows time-dependent changes of the clot average deformation gradient tensor (DGT) at constant shear rate of 2000 and 1000 s^{-1} reaching steady state. (*b*) Relationship between the average deformation tensor norm $\langle \boldsymbol{F} \rangle$ and shear force density. (*c*) Black squares: the total volume of fragments that passed through the observation cross section Γ; red diamonds: the total volume of individual platelets accumulated on the clot; blue open squares: the total volume of individual platelets detached from the surface of the clot; (*d*) Mean velocity of plasma in the core (red closed symbols, right *y*-axis) and shell regions (black open symbols, left *y*-axis) as functions of inlet velocity. (Online version in colour.)

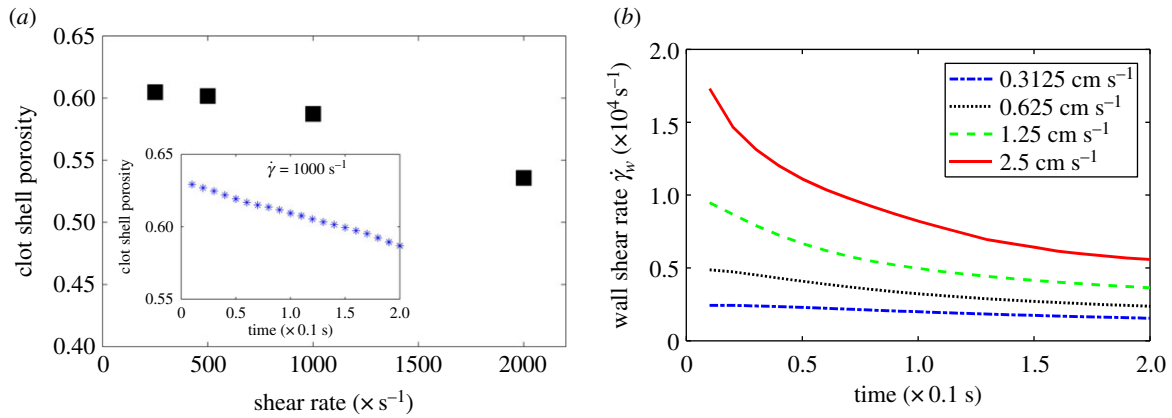

Figure 7. (*a*) Changes in clot shell porosity with flow shear rate. Inset indicates time-dependent variations in clot porosity at the shear rate of 1000 s^{-1}. Here, macroscale deformation of a clot is almost not noticeable at $t = 0.2$ s. (*b*) Time-dependent changes of the maximum local wall shear rate assessed on the vessel wall opposite to the clot for different inlet shear rates. The Inset contains schematic diagram of wall shear rate. The clot shell permeability is $K_s = 10^{-12}$ m^2. The shell porosity is the volume average of the porosity $(1 - \phi_3)$ in the shell region. ϕ_3 is redistributed due to the compression and shear (figure 5). Simulation show that the volume average of the clot in the shell region increases due to the platelets moving along the direction of the flow. (Online version in colour.)

velocities. This discrepancy can be attributed to the fact that our model accounts for the reduction in clot porosity during its deformation in response to shear flow, while in [11] these effects were omitted and instead the flow through a non-deformable clot of constant porosity was modelled. Since clot deformation and internal flow dynamics are coupled, accounting for their relation makes our model more realistic and enables simultaneous evaluation of nonlinear structural changes and transport properties of the clot under flow.

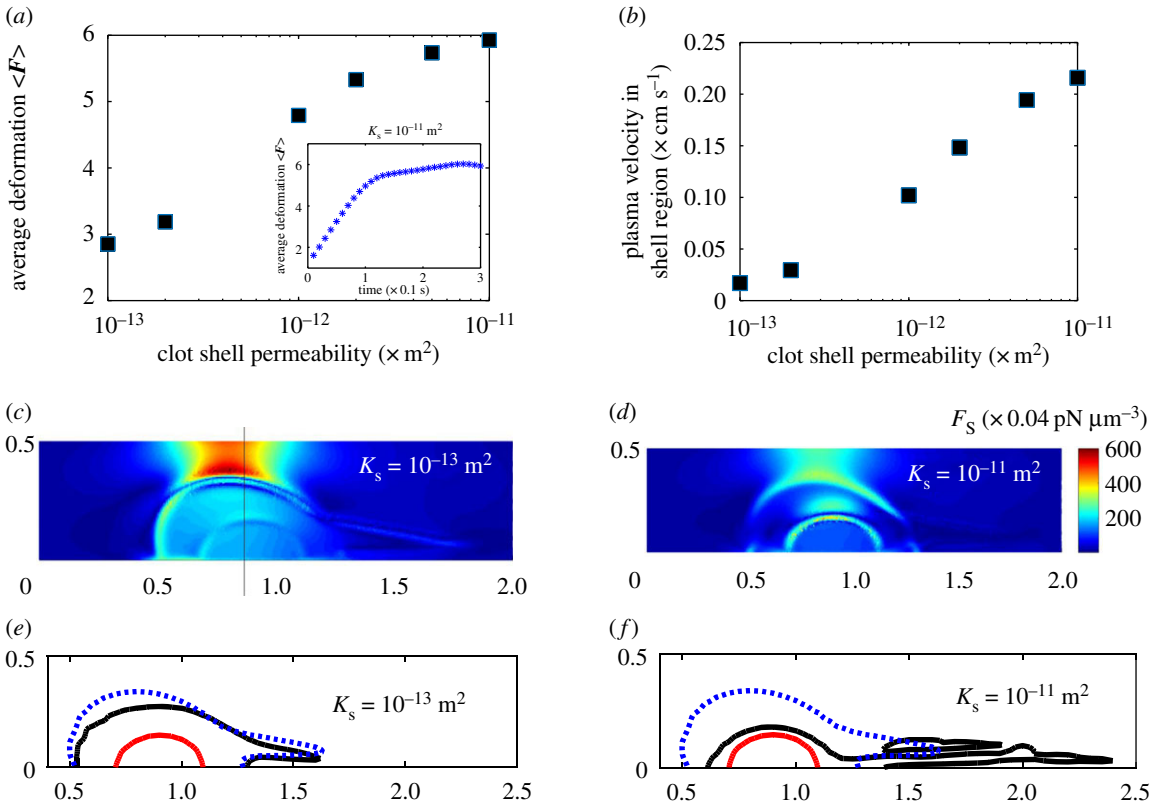

Figure 8. Effect of clot permeability on clot deformation, fragmentation and flow dynamics. (*a*) Volume averaged deformation tensor norm $\langle \boldsymbol{F} \rangle$ as a function of clot shell permeability. The inset shows the evolution of the average deformation gradient tensor (DGT). (*b*) Relationship between mean plasma velocity in the clot shell region and shell permeability. (*c,d*) Spatial distribution of the shear force density induced by the flow over the clot with shell permeability $K_s = 10^{-13}$ m^2 and $K_s = 10^{-11}$ m^2, respectively, at time $t = 0.001$ s. (*e,f*) Flow-induced deformations of blood clots with shell permeability $K_s = 10^{-13}$ m^2 and $K_s = 10^{-11}$ m^2 at flow shear rate of 1000 s^{-1} at time $t = 0.3$ s. The black curve outlines the surface of the blood clot and its fragments. The red curve depicts the interface between the core and shell regions. The blue dot lines indicate initial interfaces. The unit of lengths are in terms of $L = 100$ μm (figure 3). (Online version in colour.)

5.2. Effect of the flow shear rate on clot integrity

Simulations revealed two mechanisms by which shear rates affected the size of dislodged clot fragments: (i) a ratio between formation and breakage of the weak bonds between individual platelets and between platelets and clot surface that stabilize the size of the clot, and (ii) tearing pieces off the clot shell. To quantify the second mechanism, we tracked aggregates of platelets passing across a selected cross-section area Γ of the simulation domain on the downstream side of the blood clot (figures 3*c* and 5*a–d*). Specifically, Γ was positioned at $x = 2.5L$ of the simulation domain, where $L = 100$ μm. Only aggregates that were detached and carried by the flow through Γ were evaluated and the total size of pieces was assessed. Platelets in simulations get removed or detached from the surface of a clot due to continuous peeling of small platelet aggregates and tearing of larger pieces off the clot. Tearing, resulting in the volume fraction of clot material detected by the filter at Γ, larger than 0.25, $\phi_3 \geq 0.25$, during 0.3 s is recognized as an event of embolization.

Figure 6*c* shows the total size of the blood clot pieces passing through Γ within 0.2 s, which is computed as $V_{\text{frag}} = \int_0^T \int_\Gamma \phi_3 u_1 \, \mathrm{d}A \, \mathrm{d}t$, where ϕ_3 is the clot volume fraction, u_1 is the x-component of the flow velocity, T is the observation time. At low shear rates (250 s^{-1}) no pieces of the clot passed through Γ. At $\dot{\gamma} = 500$ s^{-1}, larger portions of the blood clot began to pass through the observation section Γ. As the flow shear rate increased further, a linear increase of V_{frag} was observed (figure 6*c*). Comparison of the clot portions' size detached from the clot by flow revealed that the total size of clot fragments detached from the clot as individual platelets or tiny platelet aggregates were approximately five times smaller (figure 6*c*) than the size of fragments associated with flow-induced tearing off pieces of the clot shell, emphasizing the later process as a major contributing mechanism of embolization. Nevertheless, our results show that continuous microembolization takes place when a clot is subject to shear flow and this is an indispensable mechanism that limits further clot growth. From a pathogenic viewpoint, any newly formed clot is embologenic with the clinical consequence depending on the size of continuously formed emboli.

5.3. Relationship between clot permeability and its mechanical stability

Clot permeability is an important characteristic describing the ability of liquid to pass through the clot. It depends on clot structure, which is related to the tightness of cellular and fibrin packing [9,60,66]. To evaluate whether variations in clot permeability affect clot stability, we have simulated clot deformation dynamics and embolization as the permeability of the shell region varied from 10^{-13} to 10^{-11} m^2 while the core of the clot was assumed to have a low and constant permeability (10^{-14} m^2) [11,60]. Notice that we assume that clot permeability depends only on the platelet activation level. The shear rate is fixed to be 1000 s^{-1}.

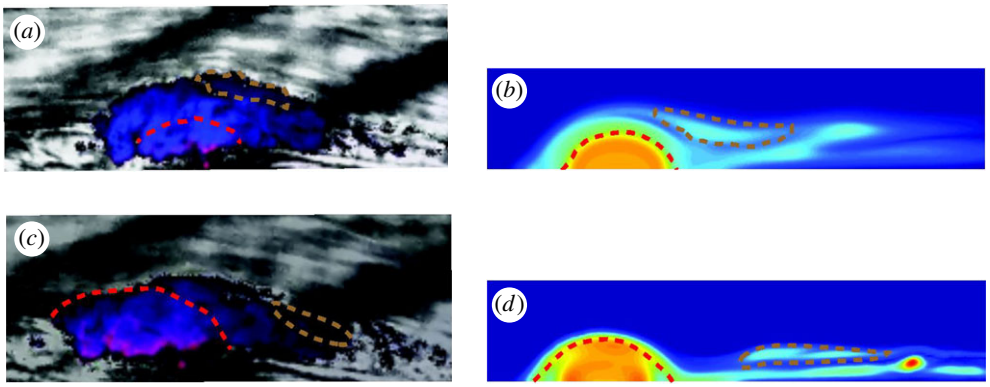

Figure 9. Predictive simulations of blood clot fragmentation dynamics and their comparison with snapshots of experimental movie (movie is provided as a supplementary information to [10]). (*a*) and (*c*) show intravital microscopy data at $t = 68$, 74 s [10]; (*b*) and (*d*) are simulation results at $t = 0.1$, 0.3 s. The core–shell interface of the clot is outlined by the red line; a clot fragment detached from the clot due to rupture is indicated by the brown dashed-line. The clot shell permeability was $K_s = 10^{-11}$ m^2. (Online version in colour.)

Table 2. Flow-induced clot volume dynamics for various clot permeability values under the blood flow with the shear rate $\dot{\gamma} = 1000$ s^{-1}. Here $L = 100$ μm.

permeability of the clot shell (10^{-13} m^2)	volume of accumulated platelets ($0.001 \times L^3$)	volume of detached platelets ($0.001 \times L^3$)	total fragment volume ($0.001 \times L^3$)	ruptured fragment volume ($0.001 \times L^3$)
100	3.2	3.1	18.1	8.5
50	3.1	3.0	15.1	5.3
20	3.1	3.4	12.4	0
10	3.4	3.8	11.2	0
2	3.9	4.5	8.4	0
1	4.1	5.3	7.4	0

The deformation of the clot at various permeabilities that was quantified in terms of the volume-average DGT $\langle F \rangle$ revealed a onefold increase in the degree of clot deformation as the shell permeability K_s increased from 10^{-13} to 10^{-11} m^2 (figure 8*a*). Accordingly, the calculated flow velocity through the shell region of the clot revealed a 10-fold increase as the clot became more permeable (figure 8*b*). To quantify clot disintegration dynamics, the volume of platelets accumulated on and removed from the surface of a clot and the volume of large clot pieces detached from the clot and passing the observation cross section Γ are given in table 2.

Model-based predictive simulations indicated that as the shell became more permeable the clot embolization rate due to the individual platelet detachment from the clot surface decreased (table 2). This can be attributed to the fact that the shear stress on the surface of the shell is lower for more permeable clots (figure 8*c*,*d*), which reduces the rate of platelet detachment from the top clot surface, due to the mechanism described by the rate function S_g characterizing differences in fluxes of attached and detached platelets on the clot surface (see §4.3).

Meanwhile, the total size of clot portions detached from a more permeable clot ($K_s = 10^{-11}$ m^2) due to tearing pieces off the clot and carried by the flow downstream through Γ was about 140% larger than the size of clot pieces detached from a less permeable clot ($K_s = 10^{-13}$ m^2) (table 2). Figure 8*e*,*f* illustrates that at time $t = 0.3$ s elongated structures detach from the more permeable clot via rupture, whereas the less permeable clot remained stable. The final size (or mass) of a blood clot with the permeability of 10^{-11} m^2 got smaller by 23% than the one with the permeability of 10^{-13} m^2. These results indicate that clots with a higher permeability are more prone to mechanical break up resulting in large emboli due to clot rupture. The simulation results are in good agreement with the experimental observations of clot deformation, formation of large emboli via break-up of the shell region, and subsequent clot stabilization obtained using intravital microscopy performed in an arteriole of a mouse [10] (figure 9).

Although permeability of the clot was shown to modulate transport of procoagulants and platelet activators such as thrombin [9], our simulations quantified flow-induced porosity changes of the clot, which have not been considered previously. Our simulations showed that as the flow shear rate increased from 250 to 2000 s^{-1}, porosity of the clots decreased by 10%, yielding an order of magnitude decrease in the average flow velocity inside the clot (figure 7*a*). In addition, following time lapse of clot porosity also revealed a gradual decrease in porosity with time (figure 7*a*, inset). Therefore, flow-induced clot deformations are accompanied by reduction of clot permeability, suggesting retardation of convective transport of blood clotting factors through the clot, which has important pathogenic and therapeutic consequences as the intrathrombous transport of pro- and anticoagulants as well as thrombolytic agents would be reduced by the smaller pore size.

It is noteworthy that with a rising shear rate the flow shear stress at the vessel wall opposite to the clot decreased by two to three times in response to a decrease of clot thickness as the clot was flattened and stretched in the direction of flow

(figure 7*b*). Reduction of the wall shear stress near the clot surface would decrease platelet activation and therefore should play an important role in preventing clot growth [9,55].

5.4. Clinical implications

Despite the tremendous clinical significance of the thromboembolism due to a high mortality rate, it remains one of the least understood consequences and complications of thrombosis. Little is known about deformability and fragility of thrombi that underlie the mechanical breakage of blood clots in response to hydrodynamic forces. Our model provides a fundamental basis for understanding the complex relationship between clot composition, mechanical properties of its components, permeability, and blood flow with varying shear rates.

Our results predict that shear flow induces continuous microembolization of an intravascular clot and that this is an indispensable mechanism that limits further clot growth and, at the same time, can result in the thromboembolism. Thus, any newly formed clot could be classified as embologenic depending on the size of continuously formed emboli. Another important clinical implication of our model simulations is the detailed description of the impact of flow shear on the clot deformation or compactization. Simulations showed that flow-induced clot deformations and clot permeability reduction occurred at the same time. Since permeability reduction leads to a slowdown of convective transport of blood components including thrombolytic agents through the clot, it is a biomedically important result.

6. Discussion of model limitations and future extensions of the model

The mechanism of platelet deposition and removal represented in our model by the empirical function S_g is shown to be in general agreement with the results of Wang *et al.* [32,33], since simulations demonstrated platelet attachment to the upstream portions of the surface of a clot and detachment from its downstream surface. Wang *et al.* [33] also found that platelets were rolling mostly on the upstream side of the clot surface while tethering/detaching platelets were primarily found on the downstream side, leading to clot continuously changing its shape. The microscale transient flipping and rolling behaviour of individual platelets are not considered in our current model, but will be incorporated into our future model by introducing spatially distributed coefficients of S_g for specific types of clot surface–platelet interactions in the presence of RBCs. An approach similar to the one described in [32,33] can also be applied for a more detailed description of platelet–clot interactions involving platelet αIIbβ3 integrin–fibrin(ogen) binding/unbinding [34,63].

The main focus of our current paper is the study of the role of clot permeability. Wang *et al.* [32,33] limit quantification of platelet–clot interactions to the case of impermeable clots. We plan to extend our model by adding detailed description of individual platelet–clot surface interactions and compare maps describing where individual platelets are expected to join the surface of the clot, obtained for permeable and impermeable clots. We already demonstrated that with an increase of clot permeability, the flow velocity component normal to the clot's surface increased, which could enhance platelet attachment to the upstream side of the clot and their detachment from or rolling over the downstream side of the clot. Therefore, we expect that changes in clot permeability would have strong impact on the map.

Because RBCs were not present in the data for *in vivo* clots used for validation of our model [10], we neglected the presence of RBCs inside simulated clots. Large *in vivo* clots usually contain a significant amount of RBCs. In this case, the blood flow profile, platelet accumulation location and rate depend on the Fahraeus–Lindqvist effect [67], and interactions between RBCs and platelets cannot be omitted [32]. Our modelling framework can be extended to account for this effect and include RBC and platelet interactions by introducing a new phase representing RBCs and making viscosity, elasticity, growth rate and permeability of the clot dependent on the RBC concentration.

Figure 5 demonstrates qualitative agreement between simulation results and experiments. There is a difference between time scales of the simulation results and experimental data presented in figure 5, on the order of minutes. The goal of our paper is to show that a novel multi-phase model is capable of capturing the dynamics of emboli formation and detachment. In future, we will extend the model to take into account additional biological details,

1. contraction of blood vessel and interaction between vessel and clot;
2. permeability changes due to rearrangement of platelets; and
3. rolling and flipping of platelet on the surface of a clot,

which will result in more biologically realistic time scale.

Finally, the current 2D computational model of deformation and embolization of a small clot formed in the arteriole can be extended to simulate mechanics of 3D clots by adding an extra transport equation describing the deformation gradient tensor $\boldsymbol{F}$ (electronic supplementary material, A.4.) [68].

7. Conclusion

Multi-phase 2D continuum three-phase model was developed to examine the mechanical stability of blood clots under various physiologically relevant flow conditions and with varying clot permeability. The model takes into account interactions between the main blood clot components, including fibrin, highly and partially activated platelets, liquid plasma, as well as elastic and viscous properties of the clot components. Verification and calibration of the model were conducted by comparison with published experimental and simulation data on an *in vitro* clotting model. Our simulation results suggest that various shear rates induce changes in clot size via two mechanisms, namely (i) relative formation and breakage of weak bonds between individual platelets and the surface of the clot, and (ii) tearing pieces off the clot (embolization). The latter mechanism is about five times more effective in modulating the size of a matured arteriolar clot. The degree of clot deformation changes nonlinearly with time and the clot becomes stiffer as its deformation increases in response to flow. Clot stiffening, associated with increased platelet density in the shell domain of the clot, reduces the degree of clot deformation. It is also demonstrated that clots with lower permeability are less deformable and less prone to shear-induced embolization.

The model can be extended further for studying clots with more complex structure which would include red

blood cells and other blood components. Model predictions can be used in future for assessment of clot mechanical stability and to predict the risk of thromboembolism under specific local haemodynamic conditions. The novel model described in the paper also expands the multi-phase modelling approach for studying biomechanics of highly deformable biological gels and biofilms of complex composition and variable permeability.

Data accessibility. Codes and several simulation movies could be found at: https://www3.nd.edu/~zxu2/blood_clot_proj.html.

Authors' contributions. J.W.W., R.I.L., O.V.K., Z.X. and M.A. designed and supervised the study. S.X. and Z.X. developed modelling and numerical approaches and conducted model simulations. O.V.K. and R.I.L. provided interpretation of the experimental data for model calibration. All co-authors analysed model simulations and wrote the manuscript.

Competing interests. We declare we have no competing interests.

Funding. This work was supported by the NIH grant no. UO1 HL116330 (S.X., Z.X., O.V.K., R.I.L., J.W.W., M.A.), National Science Foundation grant DMS-1517293 (S.X., Z.X.), American Heart Association grant 17SDG33680177 (O.V.K.), and the Program for Competitive Growth at Kazan Federal University (R.I.L.).

References

1. Campbell RA, Overmyer KA, Bagnell CR, Wolberg AS. 2008 Cellular procoagulant activity dictates clot structure and stability as a function of distance from the cell surface. *Arterioscler. Thromb. Vasc. Biol.* **28**, 2247–2254. (doi:10.1161/ATVBAHA.108.176008)
2. Cines DB, Lebedeva T, Nagaswami C, Hayes V, Massefski W, Litvinov RI, Rauova L, Lowery TJ, Weisel JW. 2014 Clot contraction: compression of erythrocytes into tightly packed polyhedra and redistribution of platelets and fibrin. *Blood* **123**, 1596–1603. (doi:10.1182/blood-2013-08-523860)
3. Kim E *et al.* 2011 Correlation between fibrin network structure and mechanical properties: an experimental and computational analysis. *Soft Matter.* **7**, 4983–4992. (doi:10.1039/c0sm01528h)
4. Kempen T, Donders W, Vosse F, Peters G. 2016 A constitutive model for developing blood clots with various compositions and their nonlinear viscoelastic behavior. *Biomech. Model. Mechanobiol.* **15**, 279–291. (doi:10.1007/s10237-015-0686-9)
5. Gersh KC, Nagaswami C, Weisel JW. 2009 Fibrin network structure and clot mechanical properties are altered by incorporation of erythrocytes. *Thromb. Haemost.* **102**, 1169–1175. (doi:10.1160/TH09-03-0199)
6. Collet JP, Montalescot G, Lesty C, Weisel JW. 2002 A structural and dynamic investigation of the facilitating effect of glycoprotein IIb/IIIa inhibitors in dissolving platelet-rich clots. *Circ. Res.* **90**, 428–434. (doi:10.1161/hh0402.105095)
7. Xu ZL, Chen N, Shadden S, Marsden JE, Kamocka MM, Rosen ED, Alber MS. 2009 Study of blood flow impact on growth of thrombi using a multiscale model. *Soft Matter.* **5**, 769–779. (doi:10.1039/B812429A)
8. Kim O, Liang X, Litvinov R, Weisel J, Alber M, Purohit P. 2016 Foam-like compression behavior of fibrin networks. *Biomech. Model. Mechanobiol.* **15**, 213–228. (doi:10.1007/s10237-015-0683-z)
9. Kim O, Xu ZL, Rosen E, Alber M. 2013 Fibrin networks regulate protein transport during thrombus development. *PLoS Comput. Biol.* **9**, e1003095. (doi:10.1371/journal.pcbi.1003095)
10. Welsh JD, Stalker TJ, Voronov R, Muthard RW, Tomaiuolo M, Diamond SL, Brass LF. 2014 A systems approach to hemostasis: 1. The interdependence of thrombus architecture and agonist movements in the gaps between platelets. *Blood.* **124**, 1808–1815. (doi:10.1182/blood-2014-01-550335)
11. Tomaiuolo M, Stalker TJ, Welsh JD, Diamond SL, Sinno T, Brass LF. 2014 A systems approach to hemostasis: 2. Computational analysis of molecular transport in the thrombus microenvironment. *Blood* **124**, 1816–1823. (doi:10.1182/blood-2014-01-550343)
12. Babushkina ES, Bessonov NM, Ataullakhanov FI, Panteleev MA. 2015 Continuous modeling of arterial platelet thrombus formation using a spatial adsorption equation. *PLoS ONE* **10**, e0141068. (doi:10.1371/journal.pone.0141068)
13. Bark D, Ku D. 2013 Platelet transport rates and binding kinetics at high shear over a thrombus. *Biophys. J.* **105**, 502–511. (doi:10.1016/j.bpj.2013.05.049)
14. Belyaev AV, Panteleev MA, Ataullakhanov FI. 2015 Threshold of microvascular occlusion: injury size defines the thrombosis scenario. *Biophys. J.* **109**, 450–456. (doi:10.1016/j.bpj.2015.06.019)
15. Virag L, Wilson J, Humphrey J, Karšaj I. 2015 A computational model of biochemomechanical effects of intraluminal thrombus on the enlargement of abdominal aortic aneurysms. *Ann. Biomed. Eng.* **43**, 2852–2867. (doi:10.1007/s10439-015-1354-z)
16. Xu Z, Chen N, Kamocka MM, Rosen ED, Alber M. 2008 A multiscale model of thrombus development. *J. R. Soc. Interface* **5**, 705–722. (doi:10.1098/rsif.2007.1202)
17. Flamm MH, Sinno T, Diamond SL. 2011 Simulation of aggregating particles in complex flows by the lattice kinetic Monte Carlo method. *J. Chem. Phys.* **134**, 034905. (doi:10.1063/1.3521395)
18. Fogelson AL, Neeves KB. 2015 Fluid mechanics of blood clot formation. *Annu. Rev. Fluid Mech.* **47**, 377–403. (doi:10.1146/annurev-fluid-010814-014513)
19. Leiderman K, Fogelson A. 2014 An overview of mathematical modeling of thrombus formation under flow. *Thromb. Res.* **133**, S12–S14. (doi:10.1016/j.thromres.2014.03.005)
20. Flamm M, Diamond S. 2012 Multiscale systems biology and physics of thrombosis under flow. *Ann. Biomed. Eng.* **40**, 2355–2364. (doi:10.1007/s10439-012-0557-9)
21. Diamond SL. 2016 Systems analysis of thrombus formation. *Circ. Res.* **118**, 1348–1362. (doi:10.1161/CIRCRESAHA.115.306824)
22. Fogelson AL, Guy RD. 2004 Platelet-wall interactions in continuum models of platelet thrombosis: formulation and numerical solution. *Math. Med. Biol.* **21**, 293–334. (doi:10.1093/imammb/21.4.293)
23. Fogelson AL, Guy RD. 2008 Immersed-boundary-type models of intravascular platelet aggregation. *Comput. Methods Appl. Mech. Eng.* **197**, 2087–2104. (doi:10.1016/j.cma.2007.06.030)
24. Filipovic N, Kojic M, Tsuda A. 2008 Modelling thrombosis using dissipative particle dynamics method. *Phil. Trans. R. Soc. A* **366**, 3265–3279. (doi:10.1098/rsta.2008.0097)
25. Pivkin I, Richardson P, Karniadakis G. 2009 Effect of red blood cells on platelet aggregation. *IEEE Eng. Med. Biol. Mag.* **28**, 32–37. (doi:10.1109/MEMB.2009.931788)
26. Symeonidis V, Em Karniadakis G, Caswell B. 2005 Dissipative particle dynamics simulations of polymer chains: scaling laws and shearing response compared to DNA experiments. *Phys. Rev. Lett.* **95**, 076001. (doi:10.1103/PhysRevLett.95.076001)
27. Tosenberger A, Ataullakhanov F, Bessonov N, Panteleev M, Tokarev A, Volpert V. 2016 Modelling of platelet–fibrin clot formation in flow with a DPD–PDE method. *J. Math. Biol.* **72**, 649–681. (doi:10.1007/s00285-015-0891-2)
28. Leiderman K, Fogelson A. 2013 The influence of hindered transport on the development of platelet thrombi under flow. *Bull. Math. Biol.* **75**, 1255–1283. (doi:10.1007/s11538-012-9784-3)
29. Leiderman K, Fogelson AL. 2011 Grow with the flow: a spatial-temporal model of platelet deposition and blood coagulation under flow. *Math. Med. Biol.* **28**, 47–84. (doi:10.1093/imammb/dqq005)
30. Voronov R, Stalker T, Brass L, Diamond S. 2013 Simulation of intrathrombus fluid and solute transport using in vivo clot structures with single platelet resolution. *Ann. Biomed. Eng.* **41**, 1297–1307. (doi:10.1007/s10439-013-0764-z)
31. Yazdani A, Li H, Humphrey JD, Karniadakis GE. 2017 A general shear-dependent model for thrombus formation. *PLoS Comput. Biol.* **13**, e1005291. (doi:10.1371/journal.pcbi.1005291)

32. Wang WW, Diacovo TG, Chen JC, Freund JB, King MR. 2013 Simulation of platelet, thrombus and erythrocyte hydrodynamic interactions in a 3D arteriole with in vivo comparison. *PLoS ONE* **8**, e76949. (doi:10.1371/journal.pone.0076949)
33. Wang W, Lindsey JP, Chen J, Diacovo TG, King MR. 2014 Analysis of early thrombus dynamics in a humanized mouse laser injury model. *Biorheology* **51**, 3–14.
34. Wu Z, Xu Z-, Kim O, Alber MS. 2014 Three-dimensional multi-scale model of deformable platelets adhesion to vessel wall in blood flow. *Phil. Trans R. Soc. A* **372**, 20130380. (doi:10.1098/rsta.2013.0380)
35. Tutwiler V, Wang H, Litvinov RI, Weisel JW, Shenoy VB. 2017 Interplay of platelet contractility and elasticity of fibrin/erythrocytes in blood clot retraction. *Biophys. J.* **112**, 714–723. (doi:10.1016/j.bpj.2017.01.005)
36. Piechocka IK, Jansen KA, Broedersz CP, Kurniawan NA, Mackintosh FC, Koenderink GH. 2016 Multi-scale strain-stiffening of semiflexible bundle networks. *Soft Matter* **12**, 2145–2156. (doi:10.1039/C5SM01992C)
37. Kang H, Wen Q, Janmey PA, Tang JX, Conti E, MacKintosh FC. 2009 Nonlinear elasticity of stiff filament networks: strain stiffening, negative normal stress, and filament alignment in fibrin gels. *J. Phys. Chem. B* **113**, 3799–3805. (doi:10.1021/jp807749f)
38. Hudson NE, Houser JR, O'Brien T, Taylor RM, Superfine R, Lord ST, Falvo MR. 2010 Stiffening of individual fibrin fibers equitably distributes strain and strengthens networks. *Biophys. J.* **98**, 1632–1640. (doi:10.1016/j.bpj.2009.12.4312)
39. Litvinov RI, Weisel JW. 2017 Fibrin mechanical properties and their structural origins. *Matrix. Biol.* **60-61**, 110–123. (doi:10.1016/j.matbio.2016.08.003)
40. Nemerson Y. 1992 The tissue factor pathway of blood coagulation. *Semin. Hematol.* **29**, 170–176.
41. Hogan KA, Weiler H, Lord ST. 2002 Mouse models in coagulation. *Thromb. Haemost.* **87**, 563–574.
42. Stalker TJ, Traxler EA, Wu J, Wannemacher KM, Cermignano SL, Voronov R, Diamond SL, Brass LF. 2013 Hierarchical organization in the hemostatic response and its relationship to the platelet-signaling network. *Blood* **121**, 1875–1885. (doi:10.1182/blood-2012-09-457739)
43. Colace TV, Tormoen GW, McCarty OJT, Diamond SL. 2013 Microfluidics and coagulation biology. *Annu. Rev. Biomed. Eng.* **15**, 283–303. (doi:10.1146/annurev-bioeng-071812-152406)
44. Chatterjee MS, Denney WS, Jing H, Diamond SL, Beard DA. 2010 Systems biology of coagulation initiation: kinetics of thrombin generation in resting and activated human blood. *PLoS Comput. Biol.* **6**, e1000950. (doi:10.1371/journal.pcbi.1000950)
45. *Hemostasis and thrombosis: basic principles and clinical practice*, 5th edn. (Brief Article) (Book Review). 2006. *SciTech Book News*.
46. Mackman N, Tilley R, Key N. 2007 Role of the extrinsic pathway of blood coagulation in hemostasis and thrombosis. *Arterioscler. Thromb. Vasc. Biol.* **27**, 1687–1693. (doi:10.1161/ATVBAHA.107.141911)
47. Rosen ED, Raymond S, Zollman A, Noria F, Sandoval-Cooper M, Shulman A, Merz JL, Castellino FJ. 2001 Laser-induced noninvasive vascular injury models in mice generate platelet- and coagulation-dependent thrombi. *Am. J. Pathol.* **158**, 1613–1622. (doi:10.1016/S0002-9440(10)64117-X)
48. Fogelson AL, Tania N. 2006 Coagulation under flow: the influence of flow-mediated transport on the initiation and inhibition of coagulation. *Pathophysiol. Haemost. Thromb.* **34**, 91–108. (doi:10.1159/000089930)
49. Stalker TJ, Welsh JD, Tomaiuolo M, Wu J, Colace TV, Diamond SL, Brass LF. 2014 A systems approach to hemostasis: 3. Thrombus consolidation regulates intrathrombus solute transport and local thrombin activity. *Blood* **124**, 1824–1831. (doi:10.1182/blood-2014-01-550319)
50. Özkaya N. 2012 *Fundamentals of biomechanics: equilibrium, motion, and deformation*. 3rd edn. New York, NY: Springer.
51. van Kempen THS, Bogaerds ACB, Peters GWM, van de Vosse FN. 2014 A constitutive model for a maturing fibrin network. *Biophys. J.* **107**, 504–513. (doi:10.1016/j.bpj.2014.05.035)
52. Tierra G, Pavissich JP, Nerenberg R, Xu Z, Alber MS. 2015 Multicomponent model of deformation and detachment of a biofilm under fluid flow. *J. R. Soc. Interface* **12**, 20150045. (doi:10.1098/rsif.2015.0045)
53. Cahn JW, Hilliard JE. 1958 Free energy of a nonuniform system. I. Interfacial free energy. *J. Chem. Phys.* **28**, 258–267. (doi:10.1063/1.1744102)
54. Feng JJ, Liu C, Shen J, Yue P. 2005 An energetic variational formulation with phase field methods for interfacial dynamics of complex fluids: advantages and challenges. *Modeling of Soft Matter*, *The IMA Volumes in Mathematics and its Applications.* **141**, 1–26. (doi:10.1007/0-387-32153-5_1)
55. Nesbitt WS, Westein E, Tovar-Lopez FJ, Tolouei E, Mitchell A, Fu J, Carberry J, Fouras A, Jackson SP. 2009 A shear gradient–dependent platelet aggregation mechanism drives thrombus formation. *Nat. Med.* **15**, 665–673. (doi:10.1038/nm.1955)
56. Litvinov RI, Barsegov V, Schissler AJ, Fisher AR, Bennett JS, Weisel JW, Shuman H. 2011 Dissociation of bimolecular αIIb β3-fibrinogen complex under a constant tensile force. *Biophys. J.* **100**, 165–173. (doi:10.1016/j.bpj.2010.11.019)
57. Hecht F. 2012 New development in freefem++. *J. Numer. Math.* **20**, 251–266. (doi:10.1515/jnum-2012-0013)
58. Trudnowski RJ, Rico RC. 1974 Specific gravity of blood and plasma at 4 and 37 degrees C. *Clin. Chem.* **20**, 615–616.
59. Ranucci M, Laddomada T, Ranucci M, Baryshnikova E. 2014 Blood viscosity during coagulation at different shear rates. *Physiol. Rep.* **2**, e12065. (doi:10.14814/phy2.12065)
60. Wufsus AR, Macera NE, Neeves KB. 2013 The hydraulic permeability of blood clots as a function of fibrin and platelet density. *Biophys. J.* **104**, 1812–1823. (doi:10.1016/j.bpj.2013.02.055)
61. Muthard RW, Diamond S. 2012 Blood clots are rapidly assembled hemodynamic sensors: flow arrest triggers intraluminal thrombus contraction. *Blood* **32**, 2938–2945. (doi:10.1161/ATVBAHA.112.300312)
62. Robinson RA, Herbertson LH, Sarkar Das S, Malinauskas RA, Pritchard WF, Grossman LW. 2013 Limitations of using synthetic blood clots for measuring in vitro clot capture efficiency of inferior vena cava filters. *Med. Devices* (*Auckland, NZ*). **6**, 49–57. (doi:10.2147/MDER.S42555)
63. Litvinov RI, Shuman H, Bennett JS, Weisel JW. 2002 Binding strength and activation state of single fibrinogen-integrin pairs on living cells. *Proc. Natl Acad. Sci. USA* **99**, 7426–7431. (doi:10.1073/pnas.112194999)
64. Hathcock JJ. 2006 Flow effects on coagulation and thrombosis. *Arterioscler. Thromb. Vasc. Biol.* **26**, 1729–1737. (doi:10.1161/01.ATV.0000229658.76797.30)
65. Lipowsky HH, Usami S, Chien S. 1980 In vivo measurements of "apparent viscosity" and microvessel hematocrit in the mesentery of the cat. *Microvasc. Res.* **19**, 297–319. (doi:10.1016/0026-2862(80)90050-3)
66. Spero R, Sircar R, Schubert R, Taylor R, Wolberg A, Superfine R. 2011 Nanoparticle diffusion measures bulk clot permeability. *Biophys. J.* **101**, 943–950. (doi:10.1016/j.bpj.2011.06.052)
67. Galdi GP, Rannacher R, Robertson AM, Turek S. 2008 *Hemodynamical flows modeling, analysis and simulation*. Basel, Switzerland: Springer.
68. Lin F, Liu C, Zhang P. 2005 On hydrodynamics of viscoelastic fluids. *Commun. Pure Appl. Math.* **58**, 1437–1471. (doi:10.1002/cpa.20074)